J. Electrochem. Sci. Eng. **16** (2026) 3077; https://doi.org/10.5599/jese.3077

Open Access : : ISSN 1847-9286
https://pub.iapchem.org/ojs/index.php/JESE

Original scientific paper

Parameter selection of cerium oxide anodic electrodeposition on screen-printed carbon electrodes using response surface methodology for nucleic acid based biosensors

Clianta Yudin Kharismasari[1], Ari Hardianto[1,2], Muhammad Ihda H. L. Zein[3], Salma Nur Zakiyyah[1], Yeni Wahyuni Hartati[1,2,✉] and Irkham[1,✉]

[1]*Department of Chemistry, Faculty of Mathematics and Natural Sciences, Universitas Padjadjaran, Bandung 45363, Indonesia*
[2]*Study Center of Sensor and Green Chemistry, Faculty of Mathematics and Natural Science, Universitas Padjadjaran, Bandung 40132, Indonesia*
[3]*Department of Chemistry "Giacomo Ciamician", Alma Mater Studiorum, University of Bologna, Bologna 40126, Italy*

Corresponding Authors: E-mail: ✉yeni.w.hartati@unpad.ac.id, ✉irkham@unpad.ac.id;
Tel.: +62-812-2132-349

Received: October 28, 2025; Accepted: February 27, 2026; Published: March 31, 2026

Abstract

Screen-printed carbon electrodes (SPCEs) modified with cerium oxide (ceria) have attracted considerable attention due to their outstanding stability and electrochemical performance, making them promising candidates for sensor and biosensor applications. However, the anodic electrodeposition of ceria on SPCEs involves multiple parameters that may strongly influence film formation and electrochemical behaviour, yet these factors have not been systematically optimized. This study aimed to determine and optimize the key parameters affecting anodic electrodeposition of ceria on SPCEs using cyclic voltammetry (CV) and response surface methodology. All four main parameters, namely UV irradiation time, distance between the SPCE and UV lamp, cerium nitrate concentration and the number of CV cycles, significantly influence the anodic electrodeposition process of ceria, shown by the statistical analysis ($p < 0.05$). The optimized SPCE/ceria electrode exhibited improved electrochemical performance, with an average peak current of 44.158 µA and a relative standard deviation (RSD) of 2.68 %. This optimized SPCE/ceria was subsequently tested for guanine oxidation using differential pulse voltammetry with an immobilized RNA probe and produced good repeatability with an RSD value of 2.37 %. The findings underscore the importance of parameter optimization to enhance the reproducibility and sensitivity of SPCE/ceria electrodes, demonstrating their strong potential for future biosensing applications.

Keywords

Ceria layer; parameter optimization; RNA immobilization; guanine oxidation

Introduction

Electrochemical sensors and biosensors have attracted the attention of researchers to be developed because this analysis technique has advantages, such as having a low detection limit, requiring a small sample volume, and being easy to miniaturize [1,2]. In electrochemical analysis, electrodes are very important components because they play a role in electron transfer [2]. Screen-printed carbon electrode (SPCE) is a widely used electrode developed by researchers to improve its performance, one of which is modifying the SPCE surface with ceria. Ceria, or cerium oxide (CeO_2) is a rare-earth oxide extensively explored in catalysis, energy storage, and electrochemical sensing. Its redox activity, high oxygen storage capacity, chemical stability, and ability to interact with biomolecules make it a promising modifier for electrodes [3-6]. Electrodeposition of ceria on SPCE improves electron transfer, surface area, and catalytic performance, thereby enhancing the sensitivity of electrochemical systems [7-10]. To modify SPCE with ceria, the electrodeposition method offers a simple procedure, a fast process, and produces an even distribution of ceria particles [11]. In various studies on electrodeposition, cyclic voltammetry (CV) is a commonly used technique for electrodepositing metals onto working electrodes [12-14]. This technique enables simultaneous electrodeposition and redox characterization, thereby providing stepwise control over metal growth. By appropriately tuning the experimental parameters, CV can be used to establish optimal conditions for obtaining a uniform, stable metallic layer [15-17].

In performing SPCE modification, experimental design is needed to identify, evaluate, establish, and understand the factors that influence the response/results of the experiment through a statistical approach [18]. Response surface methodology (RSM) is a commonly used experimental design. RSM has three main stages: parameter selection to identify parameters with significant effects, curvature determination to predict the optimum conditions of an experiment from the curvature of the contour plot, and optimization to obtain the optimum experimental response [19,20]. These stages need to be carried out because ceria electrodeposition on the SPCE surface is certainly influenced by various factors. However, the factors that significantly influence and the optimum conditions for SPCE modification with ceria by electrodeposition are not yet known. The significance and optimization of these factors are important to know so that ceria electrodeposited SPCE can produce an optimum and consistent current response. Therefore, ceria electrodeposited SPCE can be used in sensor and biosensor applications under fixed initial conditions to improve the stability of electrode measurements.

This study discusses the selection of parameters for the modification of SPCE with ceria by anodic electrodeposition, as this stage is important for maximizing the experimental response. The parameters tested were UV irradiation time, SPCE distance to the UV lamp, cerium nitrate solution concentration, and the number of CV cycles. The selection of these parameters was carried out using the RSM experimental design with the 2-level 1/2 fractional factorial design method. The optimized SPCE/ceria was subsequently used to immobilize RNA probes via the streptavidin-biotin interaction, and the immobilization efficiency was verified by guanine oxidation measurements using differential pulse voltammetry (DPV).

Experimental

Chemicals and materials

The materials to be used are SPCE ProSens-C (PT. Maju Industri Indonesia, Figure S1.) with specifications of working electrode (WE) in the form of carbon with a diameter of 4 mm, counter electrode (CE) carbon and reference Ag/AgCl electrode (RE), cerium(III) nitrate hexahydrate ($Ce(NO_3)_3.6H_2O$)

(Merck, Germany), potassium ferric cyanide ($K_3[Fe(CN)_6]$) (Merck, Germany), potassium chloride (KCl) (Sigma Aldrich, Germany), phosphate buffer saline (PBS), TE buffer pH 8.0 (Nippon Gene, Japan), streptavidin (STV), bovine serum albumin (BSA) and biotin-RNA probe.

SPCE modification with ceria and SPCE/ceria characterization

SPCE was washed with demineralized water, then irradiated with UV light (λ = 268 nm) for several minutes at a predetermined distance between the SPCE and the UV lamp. SPCE was dipped with 80 µL of cerium nitrate solution and electrodeposited using the CV technique with a potential range of -0.1 to +1.0 V and *E* step of 0.02 V. Then, SPCE was rinsed with demineralized water and dried at room temperature. SPCE/ceria was dripped with 80 µL of 0.01 M $K_3[Fe(CN)_6]$ in 0.1 M KCl to be characterized using DPV at a potential range of -0.1 to +0.6 V, an *E* step of 0.004 V, an *E* pulse of 0.025 V, a t pulse of 0.05 s, and a scan rate of 0.008 V/s. SPCE/ceria was also characterized by SEM (JEOL JSM-IT500, Japan). This procedure is also performed on SPCE that has not been exposed to UV light beforehand.

Parameter selection

Parameter selection was performed using the R programming language through Jupyter Notebook [21-23], using the 2-level 1/2 fractional factorial design method with the selected parameters shown in Table 1.

Table 1. *Parameters affecting the experiment*

Parameter	Reference
SPCE exposure time using UV light, min	[24]
Distance of SPCE to UV lamp, cm	[25]
Concentration of cerium nitrate solution, ppm	[11]
Scan rate of CV, V s^{-1}	[26]
Number of CV cycles	[27]

Immobilization of RNA probe on SPCE/ceria and guanine characterization

A volume of 5 µL of 50 ppm streptavidin (STV) was added onto the SPCE/ceria surface and incubated for 2 hours at 4 °C. The SPCE/ceria/STV was then rinsed with PBS solution (pH 7.4) and allowed to dry. Subsequently, 5 µL of 1 µM biotin-RNA probe was added to the modified SPCE and incubated for 1 hour at 37 °C. The SPCE/ceria/STV/biotin-RNA was rinsed with TE buffer and dried before being added to a 0.01% BSA solution, then incubated for 15 minutes at room temperature. After rinsing with PBS (pH 7.4) and drying, characterization was performed using DPV in PBS (pH 7.4) as the electrolyte, within a potential range of 0.0 to +0.8 V, with a step potential of 4 mV, pulse amplitude of 25 mV, pulse time of 0.05 s and a scan rate of 0.008 V s^{-1}.

Results and discussion

Ceria electrodeposition and characterization

Prior to electrodeposition (EDP) of ceria and UV pre-treatment, the electrode surface was activated to ensure reproducible, homogeneous ceria deposition on the SPCE. The UV pre-treatment was applied to remove organic contaminants from the SPCE surface and introduce oxygen-containing functional groups, thereby improving surface wettability and enhancing interactions between the electrode surface and cerium species in solution. This pre-treatment step also promotes more uniform nucleation during subsequent ceria electrodeposition.

Following UV pre-treatment, ceria EDP was carried out to modify the SPCE surface with electroactive cerium oxide, aiming to enhance electron transfer properties and increase the effective electroactive surface area of the electrode. The EDP of ceria was performed using cyclic voltammetry. During the forward potential sweep toward +1.0 V, the process is predominantly anodic, involving oxidation reactions. The primary reaction is the oxidation of Ce^{3+} to Ce^{4+}, which occurs directly at the electrode interface, Equations (1) and (2) [13,28].

$$Ce^{3+} + 2H_2O \rightarrow Ce(OH)_2^{2+} + 2H^+ + e^- \quad (1)$$

$$Ce(OH)_2^{2+} \rightarrow CeO_{2(s)} + 2H^+ \quad (2)$$

Anodic electrodeposition is known to produce more homogeneous and adherent ceria layers compared to cathodic deposition techniques. Wang and Golden demonstrated that anodically electrodeposited ceria forms thinner, more uniform, and strongly adherent layers, whereas cathodically deposited ceria tends to be powdery and poorly attached to the substrate [29]. Furthermore, other studies have reported that anodic electrodeposition promotes the growth of ceria layers with preferred crystal orientation. Under optimized deposition conditions, the resulting ceria films exhibit a dominant (111) orientation rather than a random crystalline structure, which is beneficial for electrochemical applications [30].

Electrochemical characterization was carried out using DPV to assess the effect of surface modification on the electrode's electrochemical behaviour. Figure 1 compares the peak currents obtained from bare SPCE, UV-pretreated SPCE, and ceria-modified SPCE.

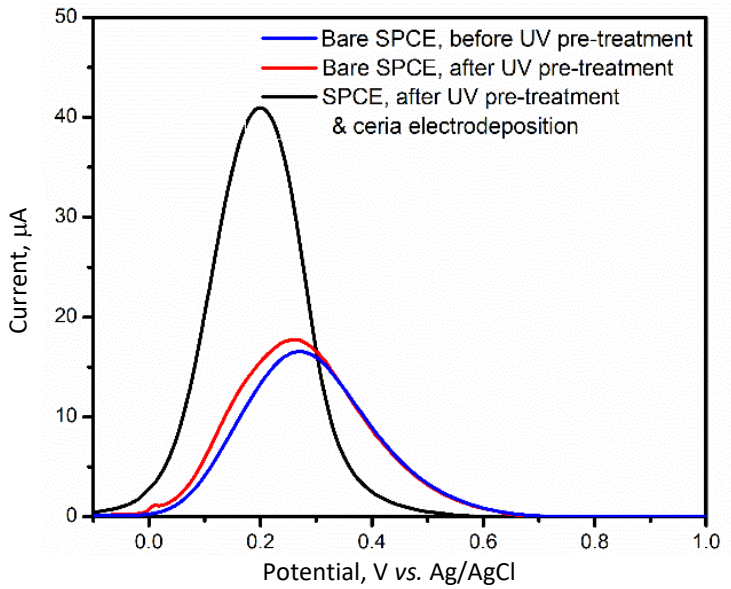

Figure 1. *DPV voltammograms of bare SPCE before UV pre-treatment (blue), after UV pre-treatment (red), and SPCE/ceria (black) with $[Fe(CN)_6]^{3-/4-}$ redox system in 0.1 M KCl solution within potential range of -0.1 to +0.6 V, potential step of 4 mV, potential pulse of 25 mV, t pulse of 0.05 s, and scan rate of 8 mV s^{-1}*

The SPCE/ceria electrode exhibits a significantly higher peak current than both the bare and UV-treated SPCEs, indicating enhanced electron transfer at the electrode interface. This improvement can be attributed to the presence of ceria on the electrode surface, which facilitates charge transport and increases the effective electroactive surface area, thereby improving the overall conductivity and electrochemical performance of the SPCE.

To further confirm the successful electrodeposition of ceria, surface morphology characterization was performed using scanning electron microscopy (SEM). Figure 2 shows the surface morphology

of the SPCE before and after ceria modification. The bare SPCE displays a relatively uniform carbon surface, whereas the ceria-modified SPCE (Figures 2c and 2d) exhibits clearly visible ceria particles distributed across the electrode surface. The deposited ceria particles have sizes in the range of approximately 1.5 to 3 µm, providing direct evidence that ceria was successfully immobilized onto the SPCE *via* anodic electrodeposition.

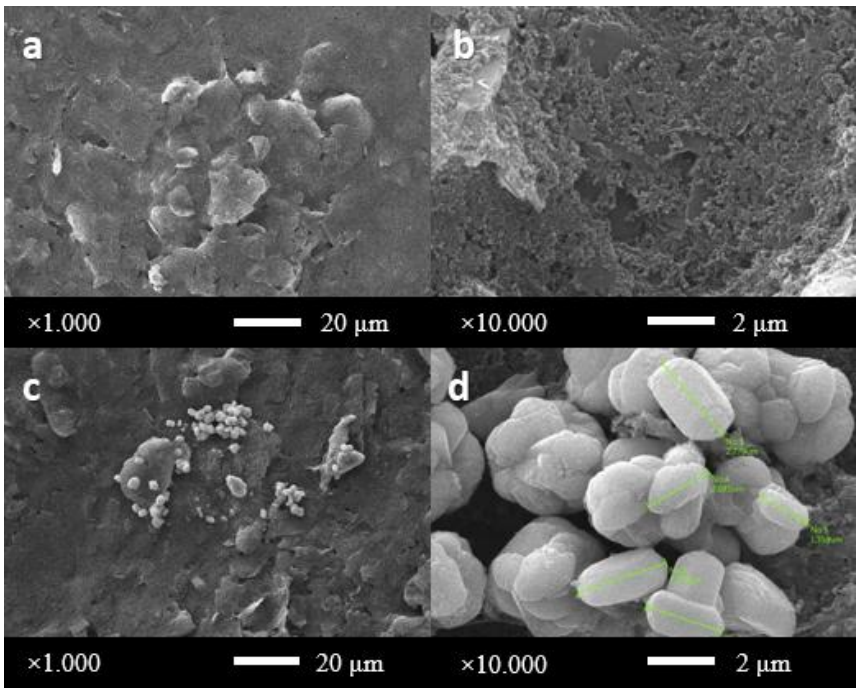

Figure 2. *The results of SPCE surface characterization using SEM: a) and b) SPCE bare; c) and d) SPCE/ceria*

In addition, the surface elemental composition of the electrodes was analysed using energy-dispersive X-ray spectroscopy (EDS). As shown in Figure 3, the ceria-modified SPCE surface consists primarily of carbon, oxygen, and cerium.

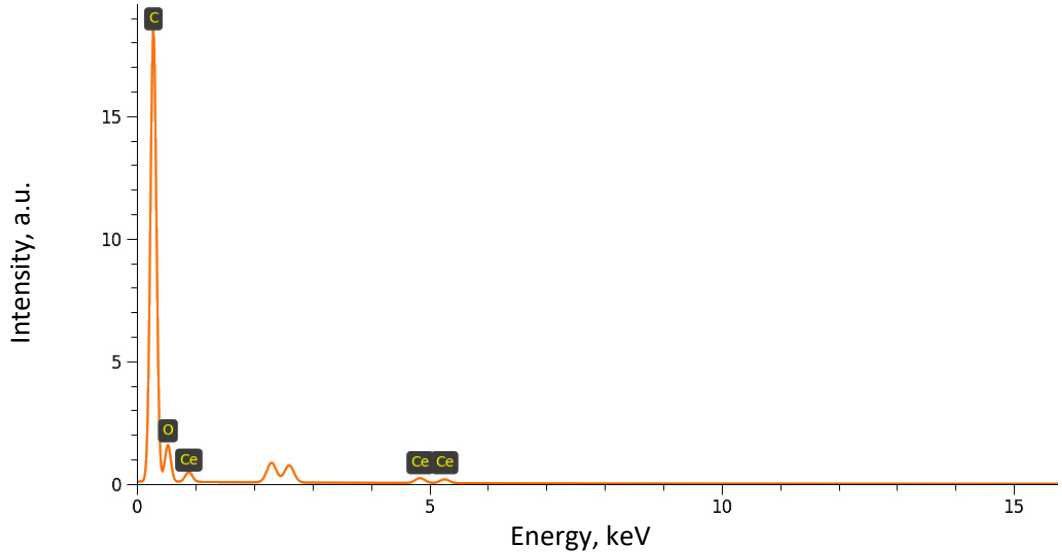

Figure 3. *Surface characterization results of SPCE/ceria using SEM-EDS*

Carbon originates from the SPCE working electrode material, while oxygen is associated with ceria as well as surface oxidation induced by the UV pre-treatment process. The presence of cerium further confirms the successful deposition of ceria onto the SPCE surface. The corresponding weight

percentages of each element are summarized in Table 2, which supports the SEM observations and confirms the effectiveness of the ceria modification process.

Table 2. *Surface characterization results of SPCE/ceria using SEM-EDS*

Element	Content, wt.%
Carbon	90.38
Oxygen	9.18
Cerium	0.43

Parameter selection

The characterization results, in the form of current peaks, are influenced by several factors during the manufacture of SPCE/ceria, such as pre-treatment of SPCE with UV light, the concentration of the cerium nitrate solution, the scan rate of CV, and the number of CV cycles. Therefore, we tested these four factors in the first stage of parameter selection, using the levels shown in Table 3. The first parameter selection was carried out using a 2-level 1/2 fractional factorial design with two replications.

Table 3*. Parameters, levels, and p-values in the first stage of parameter selection (-1 is low level and +1 is high level)*

Parameter	Level		*p*-value
	-1	+1	
SPCE pre-treatment	Yes	No	0.732
Concentration of cerium nitrate solution, ppm	100	1000	0.163
Scan rate of CV, V s^{-1}	0.05	0.1	0.931
Number of CV cycles	5	15	0.723

According to Güneş *et al.* [31], UV light can oxidize carbon to form C-OH and C-O-C bonds on the electrode. UV light is known to produce ozone (O_3) and simultaneously break down ozone into oxygen ions (O^-). These ions can react with other oxygen molecules (O_2) to produce more O_3 molecules or attack carbon to form esters, hydroxyls and carboxyls [31]. Other research also shows that UV light can produce molecules or break them down into atomic oxygen, which can slowly etch the carbon surface, forming oxygen-containing groups and thus roughening the surface [25,32]. The oxygen-containing groups on the SPCE surface make the electrode more electronegative and enhance diffusion-driven processes [25], allowing positively charged ions, such as Ce^{3+}, to diffuse more readily across the electrode surface. Furthermore, UV irradiation of carbon-based electrodes can also remove some organic binders present on the electrode surface [25].

The concentration of the cerium nitrate solution also affects the current response. The higher the solution concentration, the greater the number of ceria particles electrodeposited on the SPCE surface. This impacts the resulting peak current response. Figure 4 shows that the peak current value from a 1000 ppm cerium nitrate solution is higher than that from a 100 ppm cerium nitrate solution.

In this study, anodic electrodeposition was carried out using CV with parameters such as scan rate and number of cycles. The obtained results showed that the scan rate did not have a significant effect because ceria electrodeposition proceeds mainly through charge transfer and hydrolysis of Ce^{3+} ions, rather than diffusion-limited mechanisms [33]. The significance of the scan rate is shown in Figure 4. Figure 4 shows the peak current response data for each parameter and applied level, plotted. The further the distance from the lowest and highest points, the greater the significance of the parameter. On the other hand, the number of CV cycles was chosen as a factor because

according to research by Argoubi *et al.* [24], it affects the size of the metal nanoparticles formed during the electrodeposition process. In their study, the number of metal nanoparticles increased with the number of CV cycles. This was also confirmed in the present study, where 15 CV cycles produced a higher peak current response compared to 5 CV cycles (Figure 4).

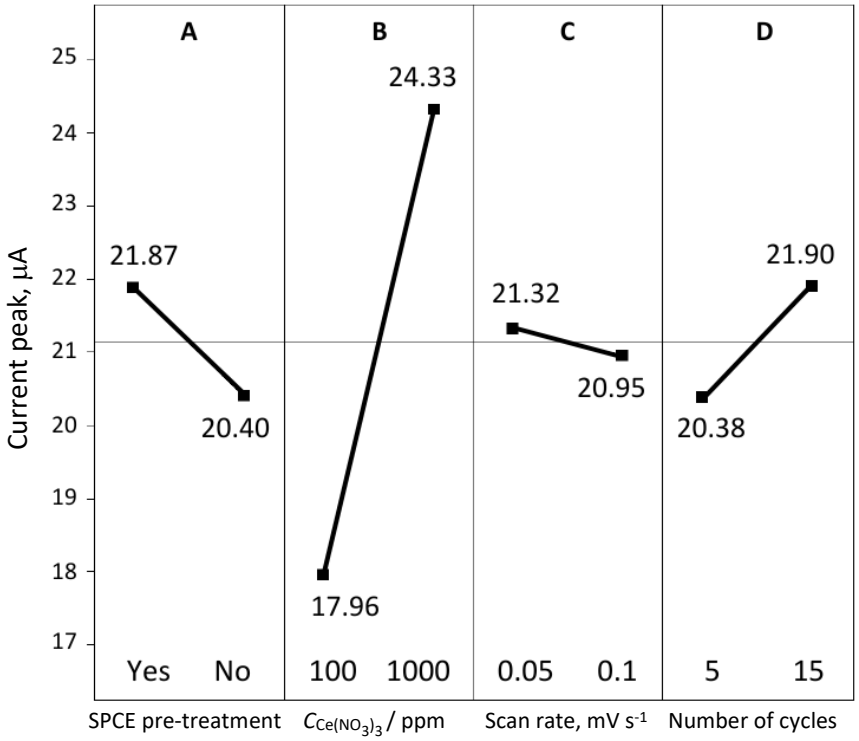

Figure 4. *Main effects plot for average peak current for first stage of parameter selection: A) SPCE pre-treatment; B) cerium nitrate solution concentration; C) scan rate; D) number of CV cycles*

At a confidence level of 95 %, the corresponding confidence intervals are expected to include the true population parameter in approximately 95 % of repeated experiments [34]. Accordingly, a p-value <0.05 was adopted as the criterion for statistical significance. However, all obtained p-values were greater than 0.05 (Table 3), indicating that none of the investigated factors exerted a statistically significant effect on the response within the tested parameter ranges. Nevertheless, analysis of the main effects plot for peak current (Figure 4) reveals clear trends in parameter levels that yield higher average current responses. Specifically, SPCE pre-treatment, a cerium nitrate concentration of 1000 ppm, a scan rate of 0.05 V s^{-1} and 15 CV cycles consistently produced higher mean peak current values. These optimal parameter levels were identified based on the calculated main effects summarized in Table S1 (Supplementary material), using experimental data obtained from the first-stage parameter screening shown in Table S2 (Supplementary material).

Parameters exhibiting levels that produced higher peak currents were selected for further evaluation in the subsequent optimization stage. To assess the influence and significance of these parameters, their levels were systematically varied. For the scan rate parameter, levels of 0.05 and 0.1 V s^{-1} yielded comparable current responses. Therefore, a scan rate of 0.1 V s^{-1} was selected for the next stage, as it enables electrodeposition to be completed in approximately half the time, thereby improving experimental efficiency without compromising performance. In this second stage, parameter selection was carried out using the 2-level 1/2 fractional factorial design method with three replications. The parameters and levels used in this stage, along with the resulting p-values, are listed in Table 4.

Table 4. *Parameters, levels and p-values in the second stage of parameter selection*

Parameter	Level		*p*-value
	-1 (low)	+1 (high)	
SPCE exposure time using UV light, min	15	60	3.38×10^{-4}
Distance of SPCE to UV lamp, cm	1.7	7.2	5.64×10^{-3}
Concentration of cerium nitrate solution, ppm	1000	2000	7.25×10^{-4}
Number of CV cycles	15	30	6.75×10^{-3}

Since UV pre-treatment of the SPCE consistently yielded higher current responses, additional UV-related parameters were introduced in the next selection stage. Specifically, UV irradiation time and the distance between the SPCE and the UV lamp were included as factors, with irradiation times of 15 and 60 min and lamp distances of 1.7 and 7.2 cm. These parameters were considered because both directly influence the physicochemical properties of the SPCE surface. Insufficient UV exposure time may lead to incomplete surface activation, resulting in sluggish electron transfer kinetics and reduced electrode sensitivity. Conversely, excessive UV irradiation can cause over-oxidation of the carbon surface, leading to the detachment of oxygen-containing functional groups and even partial structural degradation of the carbon matrix [24,35]. Similarly, placing the SPCE too close to the UV lamp increases the risk of surface heating and microstructural damage due to excessive UV intensity [36], whereas placing it too far away may result in inadequate surface activation. Therefore, both UV irradiation time and lamp distance were systematically investigated to identify conditions that balance effective surface activation and electrode stability.

Based on the peak current response data summarized in Figure 5, the average peak current at 2000 ppm is lower than that at 1000 ppm. This decrease can be attributed to the excessive concentration of cerium precursors, which promotes the formation of overly dense cerium deposits during electrodeposition. Under these conditions, cerium species tend to agglomerate, leading to the growth of larger ceria particles on the electrode surface. As a consequence, the effective surface area of ceria is reduced, thereby hindering electron transfer and lowering the electrochemical response. A similar trend is observed in the number of CV cycles. As shown in Figure 5, increasing the number of deposition cycles from 15 to 30 leads to a decrease in the DPV current response of the $[Fe(CN)_6]^{3-/4-}$ redox system. This behaviour is also attributed to excessive ceria growth and particle agglomeration at higher cycle numbers, which can partially block active sites and impede charge transfer at the electrode-electrolyte interface. These results indicate that both cerium nitrate concentration and the number of deposition cycles must be carefully optimized to balance ceria coverage and electroactive surface accessibility.

With *p*-values <0.05 (Table 4), all investigated parameters were found to have a statistically significant effect on the response. Accordingly, none of the parameters can be considered negligible, as variations across their respective levels lead to significant changes in the peak current. The significance and contribution of each factor level are illustrated in the main effects plot shown in Figure 5.

The experimental data obtained from the second-stage parameter selection are summarized in Table S3 (Supplementary material), while the calculated average peak current values for each factor and level are presented in Table S4 (Supplementary material). For SPCE exposure time under UV irradiation, a duration of 60 min yields a higher average peak current than 15 min, indicating more effective surface activation at longer irradiation times. For the remaining parameters, higher average peak currents were obtained at a SPCE-UV lamp distance of 7.2 cm, a cerium nitrate solution concentration of 1000 ppm, and a CV cycle number of 15. These conditions were therefore identified as the most favourable within the investigated parameter ranges.

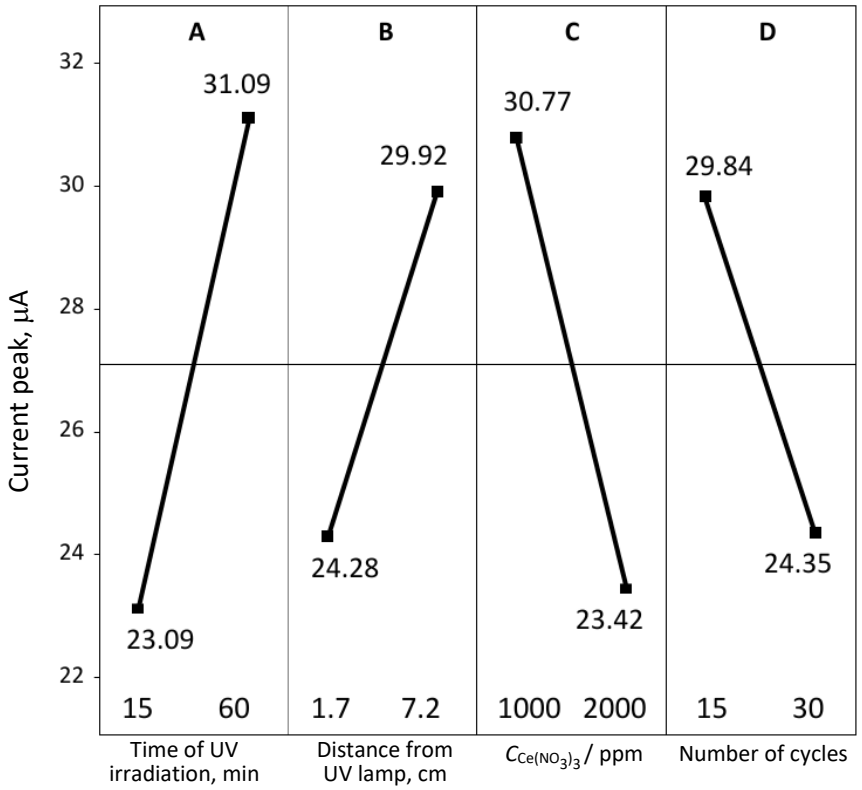

Figure 5. *Main effects plot for average peak current for the second stage of parameter selection: A) UV irradiation time; B) distance of SPCE to UV lamp; C) concentration of cerium nitrate solution; D) number of CV cycles*

To validate the parameter selection obtained from the RSM, a verification experiment was carried out by systematically varying each parameter at its non-optimal (-) level while keeping the other parameters fixed at their optimal (+) levels (Figure 6). This approach was employed to independently evaluate the contribution of each variable to the anodic electrodeposition performance. For example, to verify the effect of UV irradiation time, the SPCE was prepared under 15 min irradiation (-) while maintaining the distance to the UV lamp at 7.2 cm (+), the cerium nitrate concentration at 1000 ppm (+), and the number of CV cycles at 15 (+).

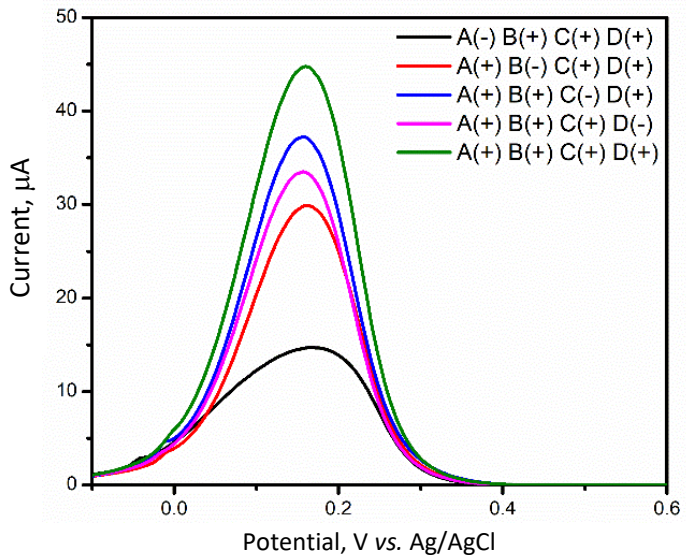

Figure 6. *Variation in peak currents as a function of each investigated parameter. DPV recorded for the* $[Fe(CN)_6]^{3-/4-}$ *redox system in 0.1 M KCl solution within a potential range of -0.1 to +0.6 V, potential step of 4 mV, potential pulse of 25 mV, t pulse of 0.05 s and scan rate of 8 mV* s^{-1}

Similar experiments were conducted for the other parameters, namely the distance between the SPCE and the UV lamp, the concentration of cerium nitrate solution, and the number of CV cycles. The results obtained are shown in Figure 6, where A is the UV exposure time, B is the distance of the SPCE to the UV lamp, C is the cerium nitrate concentration, and D is the number of CV cycles. This test was repeated three times, and the average peak current height data are shown in Table 5. The results consistently showed that SPCE prepared under the (+) levels (60 min irradiation time, 7.2 cm UV distance, 1000 ppm of cerium nitrate concentration, and 15 CV cycles) exhibited superior electrochemical performance compared to any combination containing a single parameter at its (-) level.

Table 5. *Condition of SPCE, peak current responses, average values of peak current responses and relative standard deviation (RSD) in testing the influence of parameters. I, II, and III represent the first, second and third measurements, respectively*

Condition of SPCE	Current response, µA			Average of peak current responses, µA	RSD, %
	I	II	III		
A(-) B(+) C(+) D(+)	14.703	21.970	13.362	16.678	22.67
A(+) **B(-)** C(+) D(+)	29.893	29.069	22.262	27.075	12.63
A(+) B(+) **C(-)** D(+)	37.262	37.406	31.325	35.331	8.02
A(+) B(+) C(+) **D(-)**	35.045	33.509	30.735	33.096	5.39
A(+) B(+) C(+) D(+)	45.180	44.799	42.496	44.158	2.68

The relative standard deviation (RSD, %) was calculated to evaluate the data distribution and assess the repeatability of the measurements under different SPCE conditions. As shown in Table 5, the SPCE configuration with all parameters set to the (+) level exhibits the lowest RSD among the tested conditions. This result indicates that this parameter combination provides the most consistent and reproducible electrochemical response. The low RSD observed for the (+) level configuration demonstrates that this condition not only yields higher peak-current responses but also improves measurement stability and reduces signal variability. Therefore, the combination of all parameters at the (+) level is considered optimal, as it simultaneously achieves high electrochemical performance and good data consistency, which are essential for reliable electrode preparation and subsequent analytical applications.

To demonstrate the biosensing performance of the fabricated electrode, a guanine-containing RNA probe was immobilized onto the SPCE/ceria surface. The incorporation of a guanine-rich probe enables electrochemical signal generation via guanine oxidation, thereby allowing evaluation of the electrode platform for nucleic-acid-based biosensing applications.

SPCE/ceria has been widely reported as a versatile transducer platform in electrochemical biosensors due to its excellent biocompatibility, large effective surface area, and the redox activity of Ce^{3+}/Ce^{4+} species, which collectively facilitate efficient electron transfer and stable biomolecule immobilization [6,10]. In this study, biotinylated RNA probes were immobilized onto the SPCE/ceria surface via streptavidin-biotin interactions to assess the electrode's capability for probe attachment under the optimized deposition conditions.

The biotinylated RNA probes were incubated on the SPCE/ceria surface for 1 h at 37 °C to promote effective binding. The streptavidin-biotin interaction was selected as the immobilization strategy due to its exceptional specificity and strong binding affinity [37]. With a dissociation constant (K_d) of approximately 10^{-15} M, this interaction ensures a highly stable and essentially irreversible attachment of the probe to the electrode surface [38], thereby minimizing probe desorption during subsequent washing steps or electrochemical measurements. In addition, the streptavidin-biotin system enables well-oriented and reproducible probe immobilization, which is

critical for achieving consistent biosensor performance [36-38]. Following probe immobilization, the electrode surface was rinsed with TE buffer to remove unbound probes. Subsequently, the RNA-modified SPCE was treated with 0.01 % bovine serum albumin (BSA) as a blocking agent to passivate unoccupied regions of the electrode surface [42]. This blocking step is essential for suppressing nonspecific adsorption and improving signal reliability during electrochemical measurements.

The guanine oxidation signal was evaluated using DPV to characterize probe immobilization on the electrode surface. The corresponding voltammogram is presented in Figure 7. The SPCE/ceria electrode prepared under the optimal parameter combination, which exhibited the lowest RSD, shows a higher guanine oxidation peak current and a smaller RSD (Table 6) than electrodes prepared under non-optimal conditions, characterized by higher RSD values. This behaviour indicates a greater amount and more uniform immobilization of the RNA probe on the optimized SPCE/ceria surface.

Moreover, the significantly improved reproducibility of the guanine oxidation signal at the (+) level confirms the enhanced homogeneity and surface coverage of the ceria film formed under optimized conditions. The consistent electrochemical response reflects reduced variability between electrodes, which is essential for reliable biosensor fabrication. These results demonstrate that the optimized SPCE/ceria electrode provides an excellent platform for biomolecular immobilization. Its favorable surface characteristics, combined with good electrochemical stability, make it well-suited not only for RNA probe attachment [6,8,43]. Consequently, the optimized SPCE/ceria platform shows strong potential for application in a wide range of electrochemical biosensing systems.

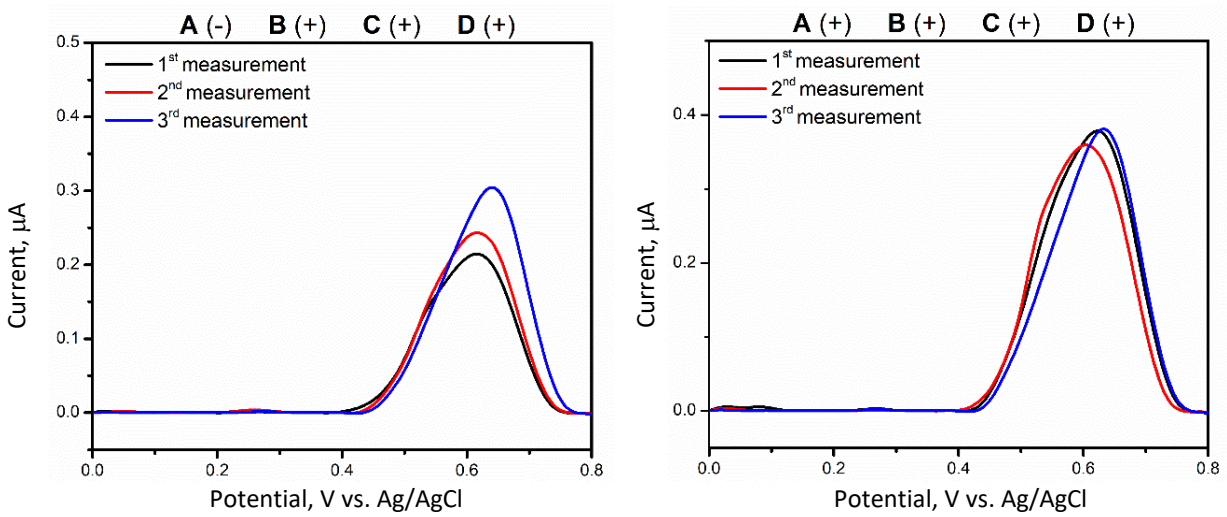

Figure 7. *Guanine oxidation peaks obtained from SPCE/ceria under non-optimal (left) and optimal (right) electrodeposition conditions. Guanine originates from the RNA probe immobilized on the SPCE surface, reflecting the electrochemical oxidation behaviour of guanine under different ceria deposition conditions. DPV recorded in PBS (pH 7.4) as the electrolyte, within a potential range of 0.0 to +0.8 V, with a step potential of 4 mV, pulse amplitude of 25 mV, pulse time of 0.05 s and a scan rate of 8 mV s^{-1}*

Table 6*. Condition of SPCE, guanine peak responses, average values of guanine peak responses and RSD. I, II, and III represent the first, second, and third measurements, respectively*

Condition of SPCE	Guanine peak response, µA			Average of guanine peak responses, µA	RSD, %
	I	II	III		
A(-) B(+) C(+) D(+)	0.218	0.246	0.306	0.257	14.30
A(+) B(+) C(+) D(+)	0.384	0.366	0.386	0.378	2.37

Conclusion

This study systematically investigated and optimized the key parameters governing the anodic electrodeposition of ceria on SPCE using cyclic voltammetry combined with response surface methodology. Four critical parameters, UV irradiation time, distance between the SPCE and the UV lamp, cerium nitrate concentration and the number of CV cycles, were identified and statistically confirmed to significantly influence the electrodeposition process (p <0.05). The stepwise parameter selection and verification approach enabled a clear understanding of how each factor affects ceria formation, electrochemical response, and reproducibility. The optimized anodic electrodeposition conditions, namely 60 min UV irradiation, a UV lamp distance of 7.2 cm, a cerium nitrate concentration of 1000 ppm, and 15 CV cycles, produced SPCE/ceria electrodes with superior electrochemical performance. These conditions yielded a high average peak current response and the lowest RSD value (44.158 µA and 2.68 %, respectively), demonstrating excellent reproducibility and uniformity of the deposited ceria layer. SEM and EDS characterization further confirmed the successful formation of ceria particles on the SPCE surface. To evaluate the practical relevance of the optimized electrode for biosensing applications, RNA probe immobilization was performed using the streptavidin-biotin interaction, and guanine oxidation was measured as an electrochemical readout. The optimized SPCE/ceria electrode exhibited a higher and more reproducible guanine oxidation signal compared to electrodes prepared under non-optimal conditions, indicating enhanced probe loading and improved surface uniformity. These results demonstrate that optimization of electrodeposition parameters plays a crucial role not only in improving electrochemical performance but also in ensuring reliable biomolecular immobilization.

Supplementary material

Additional data are available at https://pub.iapchem.org/ojs/index.php/JESE/article/view/3077, or from the corresponding author on request.

***Conflict of Interest**: The author has no conflict of interest.*

***Acknowledgements**: This research was supported by Beasiswa Unggulan Pascasarjana Padjadjaran (BUPP) of Padjadjaran University No. 996/UN6.3.1/PT.00/2025.*

References

[1] D. Grieshaber, R. MacKenzie, J. Vörös, E. Reimhult, Electrochemical Biosensors - Sensor Principles and Architectures, *Sensors* **8** (2008) 1400-1458. https://doi.org/10.3390/s8031400

[2] F.-G. Bănică, *Chemical Sensors and Biosensors Fundamentals and Applications*, John Wiley & Sons, Ltd, Chichester, West Sussex, 2012, p. 5-6. https://doi.org/10.1002/9781118354162

[3] W. X. Tang, P.X. Gao, Nanostructured cerium oxide: Preparation, characterization, and application in energy and environmental catalysis, *MRS Communications* **6** (2016) 311-329. https://doi.org/10.1557/mrc.2016.52

[4] F. Charbgoo, M. Ramezani, M. Darroudi, Bio-sensing applications of cerium oxide nanoparticles: advantages and disadvantages, *Biosensors and Bioelectronics* **96** (2017) 33-43. https://doi.org/10.1016/j.bios.2017.04.037

[5] Y. W. Hartati, S. N. Topkaya, S. Gaffar, H. H. Bahti, A. E. Cetin, Synthesis and characterization of nanoceria for electrochemical sensing applications, *RSC Advances* **11** (2021) 16216-16235. https://doi.org/10.1039/d1ra00637a

[6] R. R. Swara, N. A. Zahra, D. H. Tsary, B. A. Nania, E. Nasya, D. Setyawati, S. N. Zakiyyah, S. Ridwan, Y. W. Hartati, Porcine gelatine detection via electrochemical immunosensors utilizing green-synthesized cerium oxide nanoparticles from orange peel, *Journal of Electrochemical Science and Engineering* **15** (2025) 2698. https://doi.org/10.5599/jese.2698

[7] E. I. Fazrin, A. K. Sari, R. Setiyono, S. Gaffar, Y. Sofiatin, H. H. Bahti, Y. W. Hartati, The selectivity and stability of epithelial sodium channel (ENaC) aptamer as an electrochemical aptasensor, *Analytical and Bioanalytical Electrochemistry* **14** (2022) 715-729.
[8] Y. Nur, M.I.H. Zein, Irkham Irkham, S. Gaffar, T. Subroto, Y.W. Hartati, Cerium oxide nanoparticles-assisted aptasensor for chronic myeloid leukaemia detection, *ADMET and DMPK* **12** (2024) 623-635. https://doi.org/10.5599/admet.2404
[9] P. M. Jahani, H. Beitollahi, S. Tajik, M. R. Aflatoonian, F. G. Nejad, R. Zaimbashi, A. Mohammadnavaz, CeO_2 nanoparticles modified screen-printed carbon electrode: electrochemical sensing platform for sulfite determination in water samples, *International Journal of Electrochemical Science* **19** (2024) 100621. https://doi.org/10.1016/J.IJOES.2024.100621
[10] M. I. H. L. Zein, C. Y. Kharismasari, A. Hardianto, S. N. Zakiyyah, R. Amalia, M. Ozsoz, M. Mirasoli, Irkham, Y. W. Hartati, A CRISPR/Cas12a electrochemical biosensing to detect pig mtDNA D-loop for ensuring food authenticity, *Sensing and Bio-Sensing Research* **47** (2025) 100755. https://doi.org/10.1016/j.sbsr.2025.100755
[11] Y. W. Hartati, D. R. Komala, D. Hendrati, S. Gaffar, A. Hardianto, Y. Sofiatin, H. H. Bahti, An aptasensor using ceria electrodeposited-screen-printed carbon electrode for detection of epithelial sodium channel protein as a hypertension biomarker, *Royal Society Open Science* **8** (2021) 202040. https://doi.org/10.1098/rsos.202040
[12] J. Y. Lee, T. Tan, Cyclic voltammetry of electrodeposition of metal on electrosynthesized polypyrrole film, *Journal of The Electrochemical Society* **137** (1990) 1402-1408. https://doi.org/10.1149/1.2086681
[13] T. D. Golden, A. Q. Wang, Anodic electrodeposition of cerium oxide thin films II. mechanism studies, *Journal of The Electrochemical Society* **150** (2003) C621-C624. https://doi.org/10.1149/1.1596165
[14] E. Paradowska, K. Arkusz, D. G. Pijanowska, The influence of the parameters of a gold nanoparticle deposition method on titanium dioxide nanotubes, their electrochemical response, and protein adsorption, *Biosensors* **9** (2019) 138. https://doi.org/10.3390/bios9040138
[15] Y. Yokoyama, M. Yamamoto, K. Kano, Migration effects cause linear waveform in cyclic voltammetry of metal anode electrodeposition/dissolution without supporting electrolyte: calculations and experiments on a model case, *Electrochemistry* **92** (2024) 127002. https://doi.org/10.5796/electrochemistry.24-00108
[16] J. Lin, M. Kilani, M. Baharfar, R. Wang, G. Mao, Understanding the nanoscale phenomena of nucleation and crystal growth in electrodeposition, *Nanoscale* **16** (2024) 19564-19588. https://doi.org/10.1039/d4nr02389g
[17] A. Kaboli, N. Esfandiari, G. B. Darband, R. Sharifi, M. Aliofkhazraei, A. S. Rouhaghdam, Electrodeposition of Fe-Co-Ni coating by cyclic voltammetry for efficient hydrogen production, *Journal of Electroanalytical Chemistry* **958** (2024) 118151. https://doi.org/10.1016/J.JELECHEM.2024.118151
[18] G. Hanrahan, J. Zhu, S. Gibani, D. G. Patil, *Chemometrics and statistics | Experimental Design*, in: Encyclopedia of Analytical Science (Second Edition), Elsevier, 2005, pp. 8-13. https://doi.org/10.1016/B0-12-369397-7/00079-0
[19] R. M. Singari, Vipin, Harshit, Surface roughness prediction model for CNC turning of EN-8 steel using response surface methodology, *International Journal of Emerging Technology and Advanced Engineering* **5** (2015) 135-143. http://www.ijetae.com/files/Volume5Issue6/IJETAE_0615_23.pdf
[20] D. C. Montgomery, *Design and Analysis of Experiments*, 9th ed., John Wiley & Sons, Inc, Hoboken, N.J., 2017, p. 490-491. ISBN 978-111938-61-00

[21] U. Grömping, R package DoE.base for factorial experiments, *Journal of Statistical Software* **85** (2018) 1-41. https://doi.org/10.18637/jss.v085.i05
[22] B. E. Granger, F. Pérez, Jupyter: Thinking and Storytelling With Code and Data, *Computing in Science & Engineering* **23** (2021) 7-14. https://doi.org/10.1109/MCSE.2021.3059263
[23] I. Nurjannah, T. Subroto, A. Hardianto, L. Adinisa, K. Mochida, Key nutrient drivers for biomass and C-phycocyanin production in *Spirulina* sp. revealed by media optimization, *International Journal of Molecular Sciences* **26** (2025) 10425. https://doi.org/10.3390/ijms262110425
[24] W. R. Gallegos-Pérez, A. C. Reynosa-Martínez, C. Soto-Ortiz, M. A. Álvarez-Lemus, J. Barroso-Flores, V. G. Montalvo, E. López-Honorato, Effect of UV radiation on the structure of graphene oxide in water and its impact on cytotoxicity and As(III) adsorption, *Chemosphere* **249** (2020) 126160. https://doi.org/10.1016/j.chemosphere.2020.126160
[25] J. Wang, Z. Xu, M. Zhang, J. Liu, H. Zou, L. Wang, Improvement of electrochemical performance of screen-printed carbon electrodes by UV/ozone modification, *Talanta* **192** (2019) 40-45. https://doi.org/10.1016/j.talanta.2018.08.065
[26] N. X. Viet, Y. Takamura, Electrodeposited gold nanoparticles modified screen printed carbon electrode for enzyme-free glucose sensor application, *VNU Journal of Science: Natural Sciences and Technology* **32** (2016) 83-89. https://js.vnu.edu.vn/NST/article/download/3366/2959
[27] W. Argoubi, M. Saadaoui, S. Ben Aoun, N. Raouafi, Optimized design of a nanostructured SPCE-based multipurpose biosensing platform formed by ferrocene-tethered electrochemically-deposited cauliflower-shaped gold nanoparticles, *Beilstein Journal of Nanotechnology* **6** (2015) 1840-1852. https://doi.org/10.3762/bjnano.6.187
[28] E. Kalinina, E. Pikalova, Opportunities, challenges and prospects for electrodeposition of thin-film functional layers in solid oxide fuel cell technology, *Materials* **14** (2021) 5584. https://doi.org/10.3390/ma14195584
[29] A. Q. Wang, T. D. Golden, Anodic electrodeposition of cerium oxide thin films I. formation of crystalline thin films, *Journal of The Electrochemical Society* **150** (2003) C616-C620. https://doi.org/10.1149/1.1596164
[30] A. Q. Wang, T. D. Golden, Electrodeposition of oriented cerium oxide films, *International Journal of Electrochemistry* **2013** (2013) 482187. https://doi.org/10.1155/2013/482187
[31] F. Güneş, G. H. Han, H. J. Shin, S. Y. Lee, M. Jin, D. L. Duong, S. J. Chae, E. S. Kim, F. Yao, A. Benayad, J. Y. Choi, Y. H. Lee, UV-light-assisted oxidative sp^3 hybridization of graphene, *Nano* **6** (2011) 409-418. https://doi.org/10.1142/S1793292011002780
[32] A. Ueda, D. Kato, R. Kurita, T. Kamata, H. Inokuchi, S. Umemura, S. Hirono, O. Niwa, Efficient direct electron transfer with enzyme on a nanostructured carbon film fabricated with a maskless top-down UV/ozone process, *Journal of the American Chemical Society* **133** (2011) 4840-4846. https://doi.org/10.1021/ja108614d
[33] Y. Yang, Y. Yang, X. Du, Y. Chen, Z. Zhang, J. Zhang, Influences of the main anodic electroplating parameters on cerium oxide films, *Applied Surface Science* **305** (2014) 330-336. https://doi.org/10.1016/j.apsusc.2014.03.078
[34] S. F. O'Brien, Q. L. Yi, How do I interpret a confidence interval?, *Transfusion* **56** (2016) 1680-1683. https://doi.org/10.1111/trf.13635
[35] S. Gholipour, M. Bahreini, M. R. Jafarfard, Micro-Raman spectroscopy of graphene defects and tracing the oxidation process caused by UV exposure, *Indian Journal of Physics* **99** (2025) 1463-1469. https://doi.org/10.1007/s12648-024-03338-6
[36] F. Awaja, M. Nguyen, S. Zhang, B. Arhatari, The investigation of inner structural damage of UV and heat degraded polymer composites using X-ray micro CT, *Composites Part A: Applied Science and Manufacturing* **42** (2011) 408-418. https://doi.org/10.1016/j.compositesa.2010.12.015

[37] C. M. Dundas, D. Demonte, S. Park, Streptavidin-biotin technology: improvements and innovations in chemical and biological applications, *Applied Microbiology and Biotechnology* **97** (2013) 9343-9353. https://doi.org/10.1007/s00253-013-5232-z

[38] F. Gao, G. Liu, Y. Qiao, X. Dong, L. Liu, Streptavidin-conjugated DNA for the boronate affinity-based detection of poly(ADP-ribose) polymerase-1 with improved sensitivity, *Biosensors* **13** (2023) 723. https://doi.org/10.3390/bios13070723

[39] E. K. Hanson, R. J. Whelan, Combining the benefits of biotin-streptavidin aptamer immobilization with the versatility of Ni-NTA regeneration strategies for SPR, *Sensors* **24** (2024) 2805. https://doi.org/10.3390/s24092805

[40] E. Beitello, K. Osei, T. Kobulnicky, F. Breausche, J.A. Friesen, J.D. Driskell, Oriented surface immobilization of antibodies using enzyme-mediated site-specific biotinylation for enhanced antigen-binding capacity, *Langmuir* **41** (2025) 10576-10585. https://doi.org/10.1021/acs.langmuir.5c00656

[41] I. H. Cho, J. W. Park, T. G. Lee, H. Lee, S. H. Paek, Biophysical characterization of the molecular orientation of an antibody-immobilized layer using secondary ion mass spectrometry, *Analyst* **136** (2011) 1412-1419. https://doi.org/10.1039/c0an00672f

[42] A. Heidari, Y. J. Yoon, W. T. Park, P. C. Su, J. Miao, J. T. M. Lin, M. K. Park, Biotin-streptavidin binding interactions of dielectric filled silicon bulk acoustic resonators for smart label-free biochemical sensor applications, *Sensors* **14** (2014) 4585-4598. https://doi.org/10.3390/s140304585

[43] S. N. Zakiyyah, Irkham, Y. Einaga, N. S. Gultom, R. P. Fauzia, G. T. M. Kadja, S. Gaffar, M. Ozsoz, Y. W. Hartati, Green synthesis of ceria nanoparticles from cassava tubers for electrochemical aptasensor detection of SARS-CoV-2 on a screen-printed carbon electrode, *ACS Applied Bio Materials* **7** (2024) 2488-2498. https://doi.org/10.1021/acsabm.4c00088